AN ABSTRACT OF THE THESIS OF

Redacted for Privacy

Abstract approved:_____

William W. Warren

Crystals of CdF$_2$:In and CdF$_2$:Ga reduced in a cadmium vapor exhibit unusual metastable properties that can be explained by a "negative U" model. This work uses NMR to investigate this model for CdF$_2$:Ga and CdF$_2$:Ga,Y and compare the results to optical measurements. Temperature dependent relaxation measurements were done on ^{113}Cd in both crystals and on ^{19}F for the CdF$_2$:Ga crystal. Activation energies of 140 (10) meV for ^{113}Cd and 132 (10) meV for ^{19}F were obtained from the temperature dependent measurements. The relaxation of ^{19}F was attributed to the shallow donors while the ^{113}Cd relaxation was attributed to the concentration of electrons in the conduction band. The energies from the cadmium measurements contradict optical measurements and question the validity of the negative-U model for CdF$_2$:Ga and CdF$_2$:Ga,Y. Additionally, field dependent measurements were done on both crystals. NMR of ^{69}Ga attempted to observe the presence of the impurity for reduced and unreduced crystals. The impurity was only seen in an unreduced crystal.

NMR Studies of CdF$_2$:Ga and CdF$_2$:Ga,Y

by
Derrick J. Hilger

A THESIS

submitted to

Oregon State University

in partial fulfillment of
the requirements for the
degree of

Doctor of Philosophy

Presented July 12, 2004
Commencement June 2005

Doctor of Philosophy thesis of Derrick J. Hilger presented on July 12, 2004.

APPROVED:

Redacted for Privacy

Major Professor, representing Physics

Redacted for Privacy

Chair of the Department of Physics

Redacted for Privacy

Dean of the Graduate School

I understand that my thesis will become part of the permanent collection of Oregon State University libraries. My signature below authorizes release of my thesis to any reader upon request.

Redacted for Privacy

Derrick J. Hilger, Author

ACKNOWLEDGEMENTS

TABLE OF CONTENTS

TABLE OF CONTENTS (CONTINUED)

LIST OF FIGURES

LIST OF FIGURES (CONTINUED)

NMR Studies of CdF_2:Ga and CdF_2:Ga,Y

1. Introduction

Solid state devices are found everywhere these days, from personal computers to automobiles to small appliances to greeting cards able to record and play back sound. These devices rely on the properties of semiconductors to work. Improvements in technology and advances in the understanding of different semiconducting materials have allowed solid state devices to be come smaller, faster, and more powerful allowing them to become ubiquitous.

Most semiconductors are created by adding foreign atoms on purpose in a process called doping. Dopants can either enter the crystal lattice substitutionally for a host ion or interstitially, in an unoccupied space in the crystal lattice. In either case, the dopants are usually added to enhance electronic properties and this enhancement usually increases the number of charge carriers.

This work focuses on semiconducting cadmium fluoride, CdF_2 in crystal form. We have looked at crystals which have been doped with gallium, CdF_2:Ga, and crystals doped with both gallium and yttrium, CdF_2:Ga,Y. This work uses a technique called Nuclear Magnetic Resonance (NMR) to investigate the various electronic states of these impurities in cadmium fluoride. These crystals were

supplied by Dr. Alex Ryskin's group at the S. S. Vavilov State Optical Institute in St. Petersburg, Russia.

Section 1.1: CdF_2

Generally, solid materials can be broken down into three categories (conductors, insulators, and semiconductors) based upon the ability to conduct current. At a given temperature, an electronic conductor is a material (usually called a "metal") characterized by the presence of its highest energy electrons in a partially occupied conduction band. This allows those electrons to move about in the material. At that same temperature, an insulator has its highest energy electrons in states separated from the conduction band by an energy gap usually referred to as the band gap. A semiconductor is perhaps most closely related to an insulator. It also has a band gap. However, the band gap in a semiconductor is not as large as the gap of an insulator at the same temperature. This can make the distinction between a semiconductor and insulator nontrivial.

CdF_2, by itself, is an insulator with the atoms arranged in the fluorite structure, bonding that is very ionic and a band gap that is very large, roughly 7.8 eV (Park and Chadi, 1999). The fluorine form a simple cubic lattice with the cadmium occupying the body center of every other cube. CdF_2 can be transformed into a semiconductor by doping it with either indium or gallium and reducing with cadmium vapor. When CdF_2 is doped with indium or gallium, interstitial fluorines

form as the material self-compensates for the foreign atoms. Reducing the doped CdF_2 in cadmium vapor at high temperature removes a majority of the interstitial fluorines by essentially creating more CdF_2 as the fluorines diffuse to the surface and interact with the cadmium vapor (Kazanskii, 2000; Ryskin et al., 1995). It is these interstitial fluorines which prevent unreduced CdF_2 from being a semiconductor. Introducing yttrium in addition to gallium as a dopant is believed to increase the number of active gallium centers (Kazanskii, 2000).

Section 1.2: Bistable Defects in CdF_2:Ga and CdF_2:Ga,Y

When CdF_2 is doped with either gallium or indium and then transformed into a semiconductor in this way, interesting properties are observed. The dopants have been proposed to enter the lattice substitutionally (Ryskin et al., 1997) for cadmium and thus with an extra (unpaired) electron associated with them. However, optical and magnetic data collected at low temperature (Wilamowski et al., 1997; Ryskin et al., 1997; Ryskin et al., 1998a; Ryskin et al., 1998b) are inconsistent with properties of unpaired electrons. A different model is needed to reconcile the optical and magnetic data with the believed substitution of dopants for cadmium in the lattice.

The current model is as follows (Park and Chadi, 1999). The dopants, gallium in my work, still enter the material substitutionally for the cadmium, along with an extra electron associated with them. These gallium centers are theorized to

immediately "react" with each other such that in the ground state there are centers

with paired elections and centers without extra electrons. Due to coulombic

repulsion between like charges, there must be a mechanism for two electrons to

pair up on some sites. A lattice distortion is hypothesized to occur to account for

the energy required to pair electrons on some sites. The theoretical work done by

Park and Chadi suggests that this energy can come from a distortion in the lattice.

If gallium centers move from the body center of the fluorine cube into an adjacent

cube, enough energy is gained from the lattice distortion to pair up electrons on

some sites (Figure 1.1).
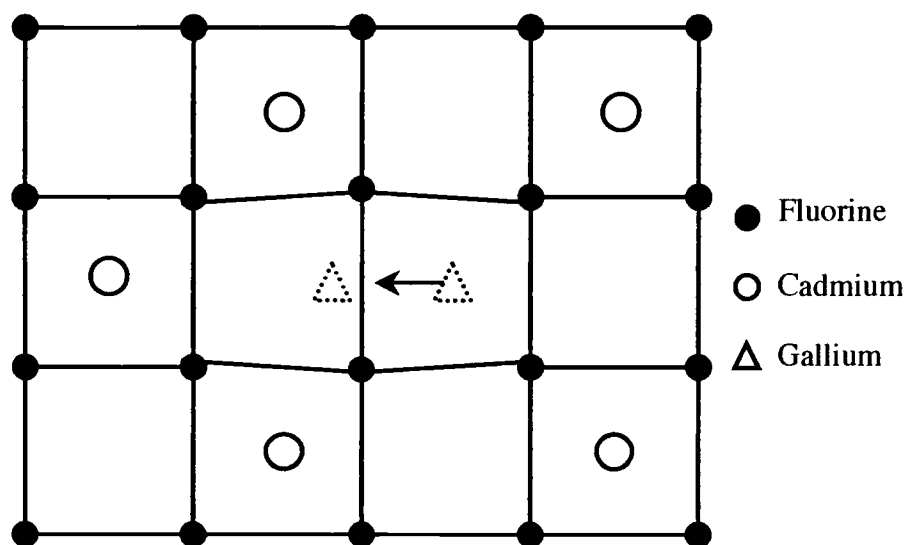
Figure 1.1: Theorized movement of cadmium after lattice distortion.

This model has a ground state in which some centers have two extra electrons and

some have no extra electrons (figure 1.2). Thermal excitations or illumination of

the material with light can drive the "reaction" between gallium centers in the

other direction. The lattice relaxes, the gallium centers have one extra electron

associated with them and are referred to as shallow donors. These electrons can easily be excited into the conduction band. The bistable nature of this model arises from low temperature optical experiments (Ryskin et al., 1997; Ryskin et al., 1998a; Ryskin et al., 1998b).
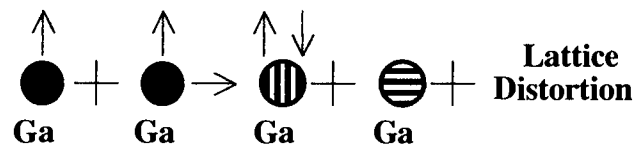
Figure 1.2: Theorized interaction between gallium centers with one extra electron each to produce sites with two extra electrons, no extra electrons, and a lattice distortion.

The excited state containing centers with unpaired spins can be "frozen in" after creating the shallow donors through optical excitation and holding the temperature below a critical value. CdF_2:In and CdF_2:Ga exhibit this bistable property, however CdF_2:Ga exhibits a higher metastable temperature (Suchocki et al., 1997; Wilamowski et al., 1997).

The bistability can be understood in terms of the configuration coordinate diagram (Figure 1.3) illustrating the theorized effect of the lattice distortion on the gallium centers and electron levels. Electrons can be excited from the doubly occupied site, or deep state, thermally or optically into the conduction band and the lattice relaxes (the gallium slides back into the body center of a fluorine cube from the face center of a fluorine cube). Then the electron will end up in a state consisting of shallow donors and centers without extra electrons.
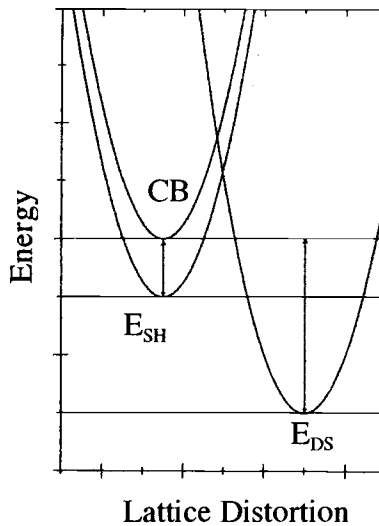
Figure 1.3: Configuration coordinate diagram illustrating the theorized lattice distortion.

These shallow donor states can be "frozen in" if optical excitations from the deep states to the shallow donor states are done at temperatures such that the thermal barrier between shallow donor state and the deep state is larger than kT. Introducing yttrium in addition to gallium as a dopant is believed to increase the number of active gallium centers (Kazanskii, 2000).

Section 1.3: Research Questions

This work uses NMR to further investigate the current model for CdF_2:Ga and the proposed effect of codoping CdF_2:Ga with yttrium. Using standard NMR pulse sequences, the relaxation of ^{113}Cd and ^{19}F can be used to investigate electronic paramagnetism in this material. As is discussed in Section 2.3, these nuclei under go nuclear spin-lattice relaxation as a result of their interactions with the unpaired spins of conduction electrons and shallow donors. Information about the energy

levels of this material can be obtained from temperature dependences of the relaxation rates. These rates can then be compared to energies obtained by optical studies done by Ruskin, Langer, and others. Similar energies between these two techniques will serve to verify the model proposed by Chadi and Chang for this material. Relaxation rates of ^{113}Cd and ^{19}F relate to the populations of electrons in the conduction band and shallow donors, respectively. The temperature dependence of the relaxation rates are related to activation energies which are functions of the energies shown in Figure 1.3. In theory, NMR can also allow for direct observation of these gallium centers and this observation will be described. This represents the first time the dopants have been seen directly in this material.

2. Theory

Section 2.1: NMR Theory

2.1.1: Zeeman Interaction

Isotopes of an element can interact with a magnetic field if they possess a magnetic moment. The Hamiltonian of this interaction is given by

$$2.1 \qquad \mathcal{H} = -\vec{\mu} \cdot \vec{B}_o$$

where μ is the magnetic moment of the isotope and $\vec{B}_o$ is the external magnetic field. The magnetic moment is related to the nuclear spin of the isotope. This relation is given by

$$2.2 \qquad \vec{\mu} = \gamma \hbar \vec{I}$$

where γ is the gyromagnetic ratio, $\hbar$ is Plank's constant divided by 2π and I is the nuclear spin of the isotope. Usually, the external field is taken to lie in the positive z direction and, as a result, the dot product in the Hamiltonian reduces to

$$2.3 \qquad \mathcal{H} = -\hbar \gamma I_z B_o$$

where I_z is the projection of the nuclear spin along the applied magnetic field. The energy eigenvalues of this Hamiltonian are

$$2.4 \qquad E = -m_z \hbar \gamma B_o$$

where m_z is a quantum number with values ranging from $I, I-1, I-2,...,-I$. The energy between adjacent levels is then given by

$$2.5 \qquad \Delta E = \Delta m_z \hbar \omega_o$$

where ω_o is called the Larmor frequency of the isotope and is given by

2.6
$$\omega_o = \gamma B_o$$

2.1.2: Bulk Magnetization in an Applied Magnetic Field

If a material containing an isotope with a magnetic moment is placed in an external magnetic field for an appropriate length of time, a bulk magnetization will be formed in the material. A bulk magnetization will be created by a population difference between the states of the individual magnetic moments. The bulk magnetization can be treated as a classical vector. The easiest example, which is true of ^{113}Cd and ^{19}F, is for $I = 1/2$ which has two possible states for the magnetic moments. These states are $I_z = \pm 1/2$ where I'll refer to $I_z = -1/2$ as "up" and $I_z = 1/2$ as "down" for reasons connected to the energy eigenvalues described in the previous section. The total magnetic moment will be given by summing up the states of each individual spin in the material, $\vec{\mu} = \sum_k \vec{\mu}_k$, where $\vec{\mu}_k$ is the moment of the kth spin in the system. The measurement of the bulk magnetization is the expectation value of the total magnetic moment, $\vec{M} = \langle \sum_k \vec{\mu}_k \rangle$. $\vec{M}$ is the thermal average of the expectation value of the total magnetic moment (Slichter, 1980).

When spins are placed in an external magnetic field and treated like classical vectors, they will precess about that field if they are initially tilted at some angle with respect to the external field. This motion (Slichter, 1980) is given by

2.7
$$\frac{d\vec{\mu}}{dt} = \vec{\mu} \times \gamma \vec{B}_o$$

If another field is created that rotates orthogonally to $\vec{B}_o$ the total field is given by

2.8
$$\vec{B}_{eff} = B_1 \cos(\omega t)\hat{i} + B_1 \sin(\omega t)\hat{j} + B_o\hat{k}$$

where $\vec{B}_o$ was arbitrarily chosen to lie along the positive z direction. The spins will

precess about an effective field in a frame rotating at frequency ω given by

2.9
$$\vec{B}_{eff} = \left(B_o - \frac{\omega}{\gamma}\right)\hat{k} + B_1\hat{i}$$

If ω equals the Larmor frequency, the only field seen by the magnetization is the

perturbing field which displaces the magnetization from its equilibrium position. If

$\vec{B}_1$ is present long enough, the spins will rotate from the positive z direction to

either the x or y direction (in the rotating frame) and will be at rest. However,

these spins will be rotating in the laboratory frame.

The precession of these spins in an external field is difficult to detect in the

laboratory because in equilibrium there is no coherence in the precession of the

spins. The lack of coherence tends to average out the changing flux created by

precessing magnetic moments. If this material is placed within an inductor

oriented perpendicular to the external field and an alternating current at the Larmor

frequency is applied for a certain amount of time, changes in the bulk

magnetization can be detected. This pulse produces a magnetic field ($\vec{H}_1$) in the

inductor and gives the precessing spins coherence by rotating the magnetization

into the x-y plane. Keeping with the classical picture of a precessing bulk

magnetization after the pulse, there will be a changing magnetic flux in the inductor.

The precessing magnetization produces a time varying flux in the inductor. This changing flux induces a voltage difference across the inductor and it's this voltage difference that can be measured and stored on a computer. If a pulse at the Larmor frequency is applied long enough to get the spins rotating coherently in the x-y plane in the laboratory frame (called a $\pi/2$ pulse), the induced voltage across the inductor will be a maximum. Not every nucleus "sees" the same local magnetic field causing there to be a range of Larmor frequencies. In this range some nuclei precess faster then the frequency of the pulse, and some precess more slowly. Over time a decay of that voltage will be seen due to this loss of coherence between precessing moments (Figure 2.1).
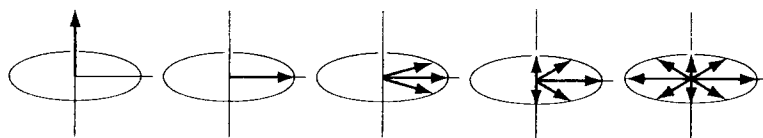
Figure 2.1: Loss of coherence resulting in an FID.

A plot of this decaying voltage is called a free induction decay (FID) (Figure 2.2). This coherent precession of magnetic moments can be detected in the laboratory.
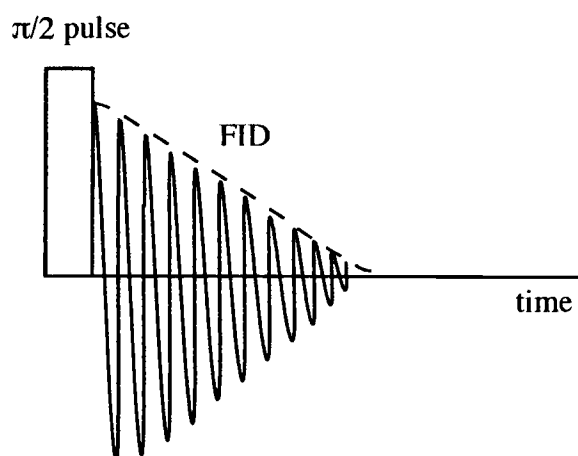
Figure 2.2: Free induction decay of an NMR signal.

2.1.3: Nuclear Quadrupolar Interaction

For nuclei with $I > 1/2$ the ion may couple with its local environment through the electric quadrupole interaction. This interaction requires a symmetry such that there exists a local electric field gradient (EFG). The EFG vanishes in places if high symmetry such as cubic symmetry, but defects or dopants can create such EFGs by lowing the symmetry. The Hamiltonian for this interaction is given by (Slichter, 1980)

$$2.10 \qquad H_Q = \frac{eQ}{6I(2I-1)} \sum_{\alpha,\beta} V_{\alpha\beta} \left[\frac{3}{2} \left(I_\alpha I_\beta + I_\beta I_\alpha \right) - \delta_{\alpha\beta} I^2 \right]$$

where $V_{\alpha\beta} \equiv \dfrac{\partial^2 V}{\partial x_\alpha \partial x_\beta}\bigg|_{r=0}$ ($\alpha,\beta = 1, 2, 3$ or x, y, z) and Q is defined to be the electric

quadrupole moment of the nucleus. Q is an operator given by

$$2.11 \qquad Q = \sum_{k}^{protons} \left(3z_k^2 - r_k^2\right)$$

where the sum is over all of the protons in the nucleus.

Section 2.2: Important Characteristic Times

2.2.1: Spin-lattice Relaxation Time (T_1)

If the population difference between the spin up and spin down states is not in thermal equilibrium, the population difference will return to its equilibrium value given enough time. The characteristic time for the bulk magnetization to return to its thermal equilibrium value is called T_1 or the spin-lattice relaxation time. The spins can go back to their equilibrium populations by exchanging energy with the lattice. For $I = 1/2$, the return of the spin populations to thermal equilibrium for an initially unmagnetized sample (just after a $\pi/2$ pulse) is given by

$$2.12 \qquad n = n_o\left(1 - e^{-t/T_1}\right)$$

where n_o is the thermal equilibrium population difference between spin down and spin up. The spin-lattice relaxation time depends on the details of the interaction between the nucleus and the lattice.

2.2.2 Free Induction Decay time (T_2^*)

The characteristic time for the FID to decay to zero is called T_2^*. Due to things such as defects in a material, not all of the spins experience the same local field. This distribution of local fields gives rise to a distribution of Larmor frequencies,

which is the main cause of the FID decay. T_2^* depends on the functional form of the decay (Figure 2.3), but the processes it describes are often reversible.
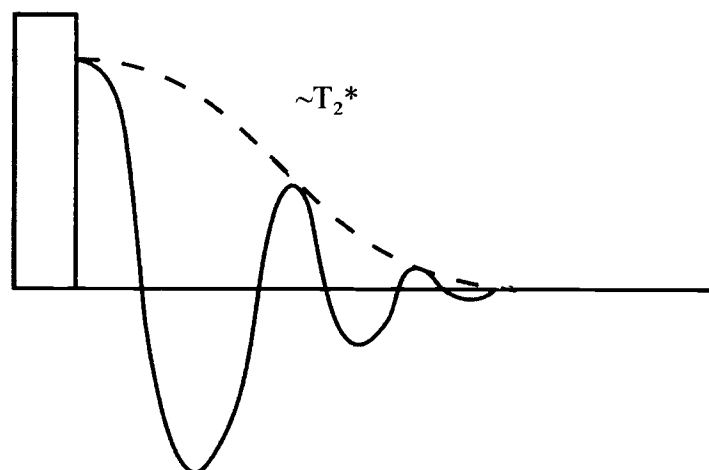
Figure 2.3: T_2^* describes the free induction decay.

Problems arise if T_2^* is too short. When a pulse is applied, physical shaking (called ringing) of the inductor occurs due to the interaction of the current with the magnetic fields. This same inductor is used to detect the bulk magnetization when the pulse ends. If the inductor is recording an FID while ringing occurs, erroneous data will be collected. To prevent the collection of erroneous data there is a "dead time" built into the software to delay the detection of the precessing magnetization. This dead time is composed of two parameters, the acquisition delay and the receiver delay, which can be set by the controlling software. The acquisition delay prevents the recording of digitization and storing of the NMR signal while the receiver delay prevents the inductor from acting like a receiver for the precessing magnetization. If T_2^* is less than the dead time of the spectrometer and T_2^* is very

short compared to T_1 then a technique called a spin echo can be used to extract the signal out of the dead time.

Application of an appropriate pulse a time τ after the $\pi/2$ pulse can cause the spins to refocus a time τ after the refocusing pulse (Figure 2.4).
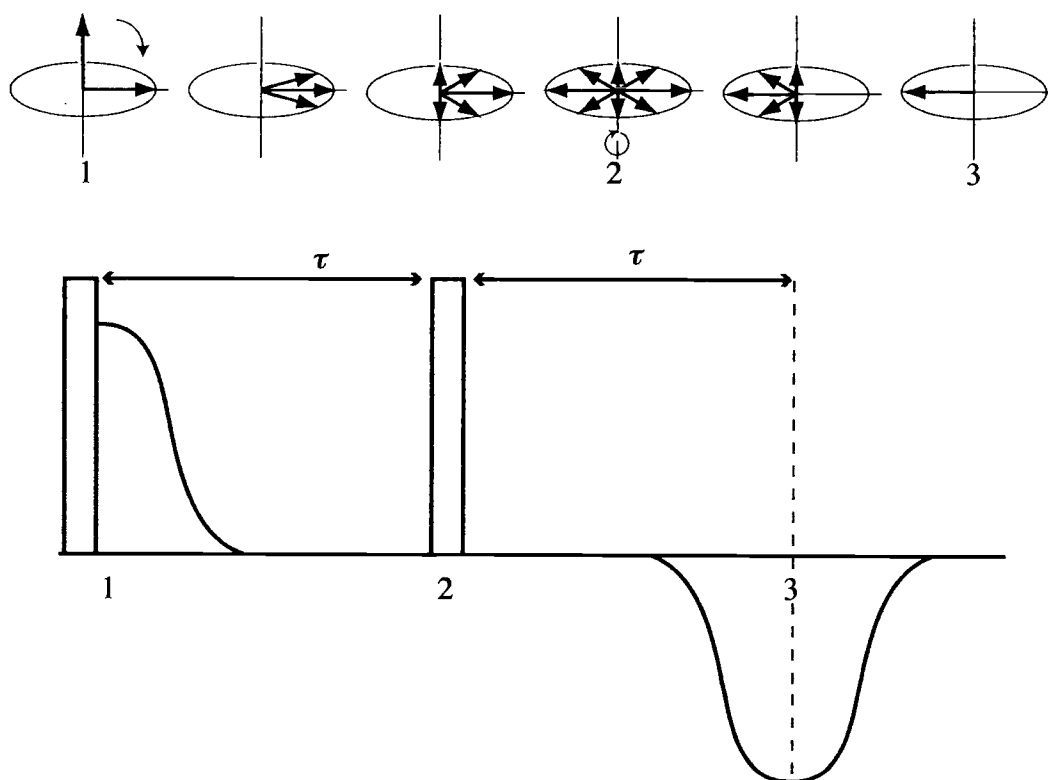
Figure 2.4: Loss of spin coherence and creation of a spin echo.

The result of refocusing the spins is called a spin echo and looks like two FIDs placed back to back. In this work a 90_x-90_y pulse sequence (Warren and Norberg, 1967) was used to create the spin echo of ^{69}Ga and thus extract the signal from the

spectrometer's dead time. ("90$_x$" means, for example, that the field producing a 90° rotation is applied along the x-axis in the rotating frame.)

2.2.3: Irreversible Transverse Magnetization Decay Time (T$_2$)

There are also times to account for other processes of the FID decay. One of the most important is T$_2$, more commonly called the spin-spin relaxation time (Fukushima and Roeder, 1981). Just as the name suggests, T$_2$ is the characteristic time for spins to interact. These processes are statistical in nature, and as a result, are not reversible like T$_2^*$ processes. To measure T$_2$, one measures the decay of the intensity of a spin echo as one increases τ (Figure 2.5).
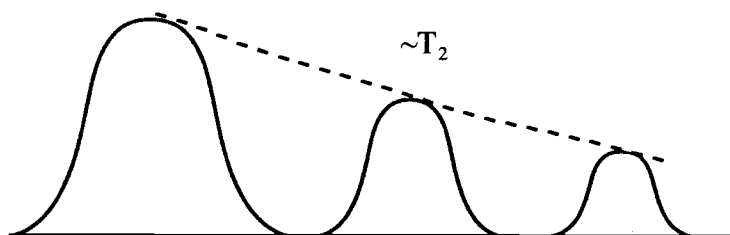
Figure 2.5: Decaying spin echoes and T$_2$.

Section 2.3 Spin Lattice Relaxation Mechanisms

Before I present a brief discussion of different relaxation mechanisms, the term "lattice" should be clarified. The term lattice in this work applies to all the reservoirs of thermal energy such as lattice vibrations, unpaired electron spins, and diffusing atoms to name a few.

2.3.1: Free Electrons in Semiconductors

Spins can return to equilibrium by exchanging energy in a variety of ways. One such way is for the spins to interact with electrons in the conduction band. These moving electrons create fluctuations in the local field seen by the moment. It is these time dependent hyperfine interactions that allow the exchange of energy to take place. We assume that the (free) electrons in the conduction band are non-degenerate and obey Boltzmann statistics, that the conduction energy band is spherically symmetric, and that the most important coupling between the electrons and nuclei is the contact interaction

2.13
$$\mathrm{H}_{\mathrm{hf, contact}} = \frac{8\pi}{3}\gamma_e\gamma_n\hbar^2\delta(r_1)(\vec{I}\cdot\vec{S}).$$

Then the relaxation rate of the nuclei is given by (Abragam, 1985)

2.14
$$\frac{1}{T_1} = \frac{64\pi}{9}N|\phi_e(0)|^4\gamma_e^2\gamma_n^2\left(\frac{m_{eff}^3 kT}{2\pi}\right)^{\frac{1}{2}}$$

Here N is the number of electrons in the conduction band per unit volume, $|\phi_e(0)|^2$ is the probability of the electron being at the nucleus normalized over the atomic volume, and m_{eff} is the effective mass of the electron. The important characteristic of this rate is that it is proportional to the number of electrons in the conduction band and to the square root of the temperature. As the number of electrons in the conduction band increases so should $\dfrac{1}{T_1 T^{\frac{1}{2}}}$.

2.3.2: Magnetic Dipolar Interaction

Spins can return to equilibrium by interacting directly with paramagnetic centers through the dipolar interaction. The direct interaction between two magnetic dipoles can be written as

2.15
$$W = \frac{\mu_o}{4\pi} \hbar^2 \gamma_I \gamma_S \frac{1}{r^3} \left[\vec{S}_I \cdot \vec{S}_S - 3(\vec{S}_I \cdot \hat{n})(\vec{S}_S \cdot \hat{n}) \right]$$

where $\gamma_{I,S}$ are the gyromagnetic ratios of the nucleus and electron, $\hat{n}$ is the unit vector in the direction of the line joining the two moments, and r is the distance between the moments (Cohen-Tannoudji, 1977). It is important to note that the interaction's strength depends on the gyromagnetic ratios and the separation distance. This is a time dependent interaction because of fluctuations of the electron spin and if we neglect any angular dependence, the relaxation rate (Abragam, 1985) is given by

2.16
$$\frac{1}{T_1} = \frac{2}{5} \frac{\gamma_s^2 \gamma_I^2 \hbar^2}{r^6} S(S+1) \frac{\tau}{1 + \omega_{Larmor}^2 \tau^2}$$

Here r is the distance between the spin (i.e. the shallow donor) and probe nucleus, ω_{Larmor} is the nuclear Larmor frequency and τ is the transverse electronic relaxation time. It is important to note that this rate is dominated by nuclei that are very close to the spin due to the $\frac{1}{r^6}$ dependence on the rate.

2.3.3: Spin Diffusion

Spins can also return to equilibrium by interacting indirectly with paramagnetic centers through a process known as spin diffusion. In this process a center that has returned to its equilibrium state and exchanged energy with a paramagnetic center "communicates" through a lattice of paramagnetic centers. Let's consider a spin one half system since both cadmium and fluorine are spin one half. Essentially, a shallow donor relaxes a neighboring ion. The relaxed ion then interacts with another neighboring ion (of the same species) through a mutual spin flip. Thus an ion not in the local environment of the shallow donor can be relaxed by the shallow donor. This process can be a major mode of spin lattice relaxation for ^{19}F in CdF_2 because ^{19}F has a large gyromagnetic ratio and is 100% isotopically abundant. This process will not work so well for ^{113}Cd because its gyromagnetic ratio is much smaller, only (roughly) 1 in 4 cadmium even have a magnetic moment and there are half as many cadmium as fluorine. Neighboring cadmiums are much farther apart than neighboring fluorines.

An excellent discussion of spin diffusion is included in Mark Shroyer's thesis (Shroyer, 1999). Only the portion relevant to this work will be discussed, but his work continues to be a great reference. The major requirement for spin diffusion is that the impurities must be far enough apart to avoid having direct interaction between them.

Consider a sphere centered at an impurity ion of radius b. In this sphere coupling between nuclei and the impurity and coupling between nuclei to neighbors of the same species can occur. In addition, the coupling between the impurity and nuclei will be stronger than if other spheres from other impurity ions are considered (nuclei in this sphere are too far away from other impurity ions and their respective spheres). The radius of this sphere in terms of the impurity concentration, N, is

$$2.17 \qquad\qquad \frac{4\pi b^3}{3} << \frac{1}{N}$$

This expression was obtained in a high temperature limit which is applicable for our range of external fields.

If the spin-lattice coupling is stronger at b than the spin-spin coupling, then relaxation by spin diffusion can only travel as fast as the magnetization can diffuse through the material. This is what is known as the diffusion limited case and the relaxation is given by

$$2.18 \qquad\qquad \frac{1}{T_1} = \frac{8\pi N D^{3/4} C^{1/4}}{3}$$

where D is the spin-spin diffusion coefficient

$$2.19 \qquad\qquad D = Wa^2$$

W is the probability of a spin flip flop between nearest neighbors, a is distance between nearest neighbors, and C is parameter describing the strength of the ion coupling given by

$$2.20 \qquad C = \frac{2}{5} \gamma_S^2 \gamma_I^2 \hbar^2 S(S+1) \frac{\tau}{1 + \omega_{Larmor}^2 \tau^2}$$

where τ is the electronic spin relaxation time and ω_{Larmor} is the nuclear Larmor frequency. Table 2.1 summarizes the important characteristics of the relaxation by spin diffusion.

Diffusion Limited $\dfrac{1}{T_1} = \dfrac{8\pi N D^{3/4} C^{1/4}}{3}$	
$\omega_{Larmor}\tau \ll 1$	$\omega_{Larmor}\tau \gg 1$
$\tau^{1/4}$	$\tau^{-1/4} B^{-1/2}$

Field and Tau Dependence		

Table 2.1: Relaxation by spin diffusion in the diffusion limited case.

2.3.4: Nuclear Quadrupolar Interaction

Relaxation through the nuclear quadrupolar interaction for spin $I \geq 1/2$ requires the electric field gradient to fluctuate over time (Van Kranendonk, 1954). These fluctuations can produce relaxation by the nuclear quadrupolar interaction even if there is a symmetry present in the crystal lattice which, if static, would produce no electric field gradient. Lattice vibrations are the most significant source of fluctuations in the electric field gradient. Relaxation through this mechanism is relevant for ^{69}Ga which possesses $I = 3/2$. ^{113}Cd and ^{19}F possess $I = 1/2$ and thus can not relax through the nuclear quadrupolar interaction.

3. Materials, Equipment and Methods

Section 3.1: Crystal Preparation

The crystals we used were grown at the Crystallography Institute of Russian Academy of Sciences in Moscow, Russia, using a modified Bridgeman technique. In this technique, a seed crystal is placed in a melt of CdF_2 containing the dopant(s). The seed crystal is slowly drawn from the melt as it grows. The doped material is an insulator at this stage, presumably due to the presence of interstitial fluorines.

The crystals were then taken to the S. I. Vavilov State Optical Institute in St. Petersburg, Russia where they were annealed at high temperature in a cadmium vapor. This process reduces the number of fluorine interstitials by essentially producing more CdF_2 as interstitial fluorines diffuse to the surface of the crystal and react with the vapor. The reduction of the interstitial fluorine makes CdF_2:Ga and CdF_2:Ga,Y semiconductors at room temperature and changes the color of the material from colorless transparency to yellowish.

The crystals used in this project were doped with a gallium concentration of $\sim 10^{19}$ cm^{-3} with the number of active dopant centers being roughly $7 \cdot 10^{17}$ cm^{-3} (Kazanskii, 2000). Codoping CdF_2:Ga with yttrium increases the number of active gallium centers (Kazanskii, 2000) from $7 \cdot 10^{17}$ cm^{-3} to $1.7 \cdot 10^{18}$ cm^{-3}. The codoped

crystals (reduced and unreduced) are cubic in shape with sides of length 4 mm. The crystals doped with only gallium are cylindrical in shape. The reduced crystal has a diameter of 5.5 mm and a length of 13.6 mm. The unreduced crystal has a diameter of 6.0 mm and a length of 14.1 mm. All of the results from our experiments were done on the reduced crystals with the sole addition of the impurity observation which was also done on the unreduced crystal.

Section 3.2: Hardware – Primary Spectrometer

Two different spectrometers were used for this project. The primary spectrometer was used for measurements where B_o was 8 T and the secondary system was used for low field measurements where B_o was 0.38 T and 0.77 T. The use of two systems was partly out of convenience and partly out of necessity. Having two spectrometers with several projects being worked on simultaneously was convenient because I could continue working on this project as long as one of the spectrometers was not being used. However, this work eventually required T_1 experiments to be carried out over a range of external fields, perfect for the secondary system.

The primary spectrometer is the CMX360-1436 from Varian, Inc. The other relevant pieces of equipment associated with the CMX are: a superconducting magnet made by American Magnetics capable of producing an 8 Tesla external field, two American Microwave Technology 3000 series linear RF power

amplifiers, an ENI 5100L NMR RF power amplifier, and a Sun Sparc10 workstation running Varian's Spinsight NMR control software on SunOS 4.1. It should also be noted that multiple amplifiers allow for double resonance and decoupling techniques to be used although these techniques were not used in this study.

Figure 3.1 shows the experimental NMR set up. Creation of an RF pulse starts with the computer telling the synthesizer the required frequency. The synthesizer produces a continuous wave at that frequency which is gated by logic circuitry to create the pulse. The pulse is then amplified and sent through eight diodes connected in parallel. Half of these diodes are connected in reverse direction. This acts as a self-activated switch to decouple the transmitter circuitry when only small signal voltages are present. The pulse goes through a directional coupler used to observe the transmitted and reflected pulses. By adjusting the tuning and matching capacitors on the probe, the ratio of the peak-to-peak voltage of the transmitted pulse to the peak-to-peak voltage of the reflected pulse is maximized. The probe is considered tuned and matched once this ratio is maximized. The tuning capacitor adjusts to the Larmor frequency of the nuclei under study while the matching capacitor adjusts to the impedance of the circuit. The signal from the nuclei present after the pulse goes from the probe through the directional coupler and through another set of diodes in parallel and connected to ground. This allows the

small signal to pass, but not the large pulses. This signal is then amplified, digitized and then stored in the computer for analysis.
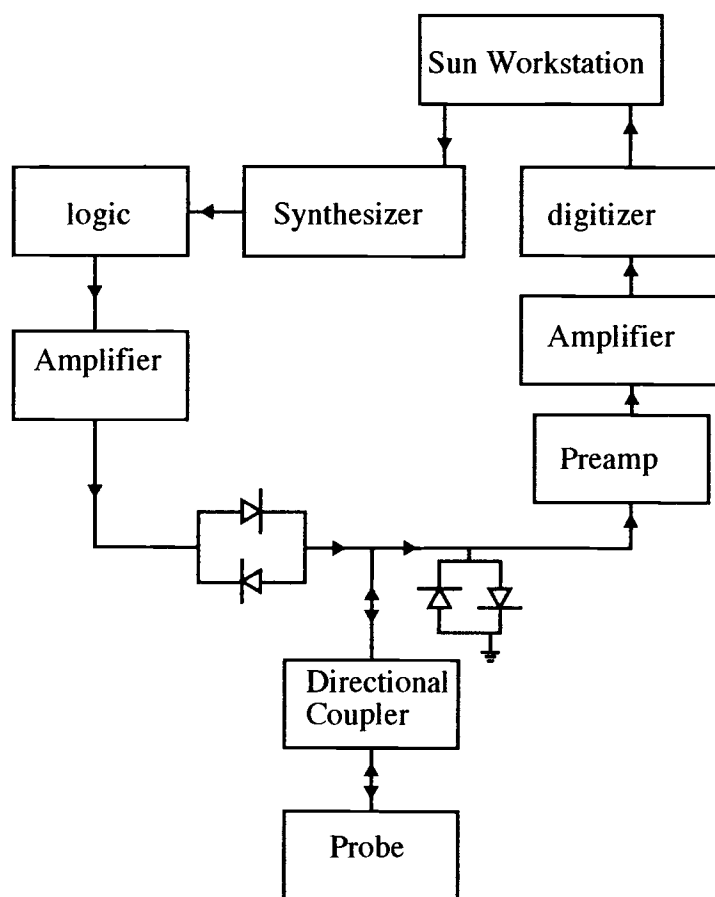
Figure 3.1: Block diagram of the NMR set up.

Variable temperature experiments were conducted on this experimental system. For experiments where 200 K < T < 400 K, a Chemagnetics RKC-REX-C1000 temperature controller and FTS Systems AirJet was used to achieve and maintain a stable target temperature. The temperature control system is precise down to a tenth of a degree Kelvin and fluctuates up or down by a tenth of a degree after the target temperature has been reached. This experimental setup requires very little

maintenance other than keeping the liquid nitrogen and liquid helium chambers above critical levels.

One disadvantage lies in measurements requiring changing the strength of the external field. The magnet is normally in persistent mode. With the magnet's Nb-Ti immersed in liquid helium, which is internally insulated by a container of liquid nitrogen, the current generating the magnetic field is able to maintain itself with very little loss over many months. Changing this current requires leads to be connected to the superconducter. As the leads are lowered into the liquid helium they will cool, but at the cost boiling of the liquid helium required to keep the magnet in persistent mode. Extra liquid helium is needed to transfer to the magnet to keep the Nb-Ti superconducting. This process can be tedious and increases the possibility of having the magnet quench.

Section 3.3: Hardware – Secondary Spectrometer

The secondary system consists of a hand built spectrometer with an electromagnet and current source capable of producing external fields in the range of $0 < B_o < 2$ Tesla. This spectrometer also is connected to an ENI A-300 RF power amplifier. This system is older and requires a more intimate knowledge of NMR than the primary system does because the setting of parameters is not done by the computer through spectrometer software communicating with the hardware. This makes the secondary spectrometer a great learning tool and, with the electromagnet, is perfect

for experiments requiring a range of external fields. However, the range of fields is limited to external fields of less than two Tesla and other hardware restrictions. No temperature dependent studies were done using this system; only field dependent studies were carried out.

3.4: The NMR Probe – The Circuit

The NMR probe is, essentially, an LC circuit. There are two capacitors in this circuit, one to match the impedance of the circuit to the $50\,\Omega$ load the spectrometer wants to see and on to tune to the resonant frequency of the nuclei. This simple circuit sits at the top of the probe (Figure 3.2) which is inserted through the bottom of the superconducting magnet.
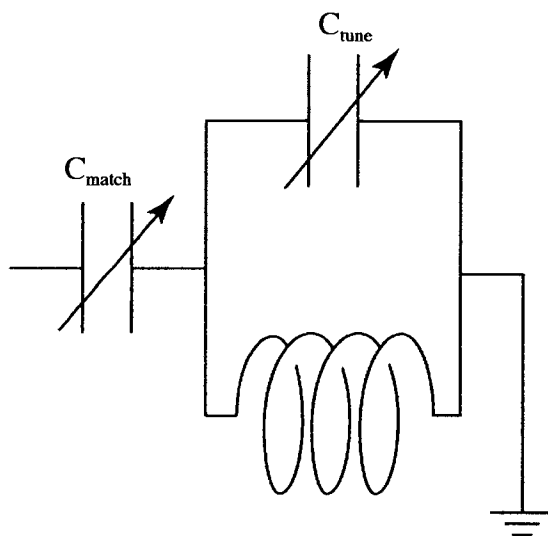
Figure 3.2: The circuit of the NMR probe.

3.5: General NMR Experimental Procedure

3.5.1: Creating the Coil from Sample Size.

Generally, the inductor that is part of the probe must be created before an experiment can be carried out. This is due to variations in sample size. If the isotope has been studied before in a known field, one can get an idea of the geometry of the inductor quickly. The geometry of the inductor is then determined by the volume of the sample and the known inductance needed to tune the circuit to the Larmor frequency of the isotope. If the isotope has not been studied before or is being studied at a different external field, things are a bit more complicated. The geometry of the inductor is still set by the dimensions of the sample. However, the inductance is unknown. I found it easiest (and less time consuming) to create inductors based on the geometry of the sample but let the number of turns vary. These inductors were then tested in the probe (without the sample) to find one that tuned to the Larmor frequency. Once such an inductor was made, I tested the inductor once more with the sample to ensure that it tuned properly with the sample in place.

3.5.2: Pulse Width Conditions

The $\pi/2$ pulse condition was found before carrying out NMR experiments in this work. As explained above, this pulse length gets the bulk magnetization rotating in the laboratory's x-y plane. Quantum mechanically this pulse equally populates the spin up and spin down states for a spin 1/2 isotope such as ^{113}Cd and ^{19}F. Another

commonly used pulse length or π pulse, which is just as its name suggests, is twice as long as the $\pi/2$ pulse. The π pulse inverts the bulk magnetization (or reverses the spin population imbalance in the quantum mechanical picture).

To find either pulse, the following procedure was used. An array in the Spinsight software was created where the width of the pulse was varied incrementally. Depending on the signal strength, multiple acquisitions were sometimes needed for each value of the pulse width in the array. The resulting FID was recorded and stored in the array. Before the next value in the array could be used, the bulk magnetization (spin populations) must return to its (their) equilibrium position (distribution). The next pulse length from the array was produced and the FID recorded followed by a wait as the system returned to thermal equilibrium. This process was repeated for each value in the array. A Fourier transform of the time domain was taken and the area under the frequency peak was calculated for each value in the array. A plot of area versus pulse width was generated and the $\pi/2$ condition was found from eyeing the resulting sinusoidal curve for the length of the pulse corresponding to the maximum area of the frequency peak. This result was checked by looking for the π condition. If the π condition was not twice as large as the $\pi/2$ condition the experiment was repeated by changing the delay between measurements. If this adjustment is necessary, it is because the sample has been saturated. This means the bulk magnetization has not been allowed to return to its equilibrium position before the next pulse was applied.

3.5.3: Measuring T_1

T_1 was measured at a given temperature and field using a standard π, π/2 pulse sequence (Figure 3.3). The bulk magnetization is inverted and after a time delay, referred to as τ, the component of the bulk magnetization along the applied field is measured using the π/2 pulse.
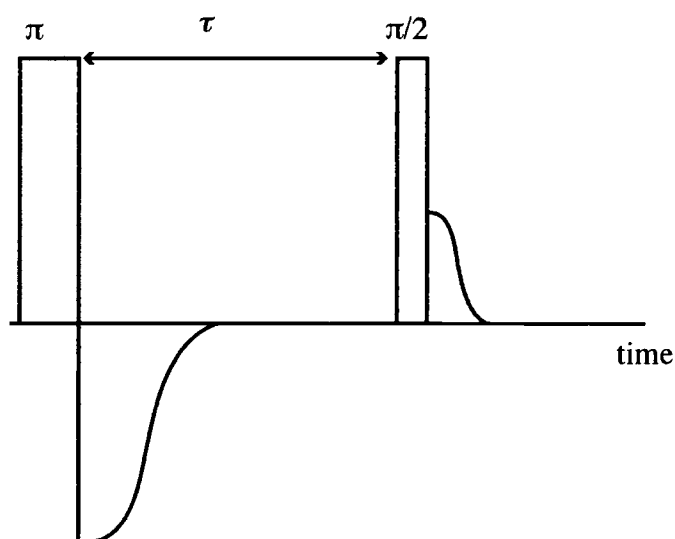
Figure 3.3: A π, π/2 pulse sequence.

To measure the strength of the recovering magnetization, an array similar to determining the π/2 condition is created where τ varies with each π, π/2 sequence. A Fourier transform of the resulting FID was calculated using the spectrometer's software. The resulting peak was integrated to quantify the strength of the recovering bulk magnetization. The magnetization is allowed to return to thermal equilibrium between after each π/2 pulse and signal averaging was used when necessary to improve the signal to noise ratio.

To measure T_1, the integral of each peak in the array mentioned above was plotted versus τ (in seconds). The resulting recovery was fit to an exponential of the form $Y = A + Be^{-kt}$ where $k = \dfrac{1}{T_1}$. These measurements took anywhere from tens of minutes to tens of hours. T_1 was measured in this way as temperature was varied and the external field was held constant for ^{113}Cd in the CdF$_2$:Ga and CdF$_2$:Ga,Y crystals. T_1 for ^{19}F was measured as a function of applied field at constant temperature for both crystals and as a function of temperature at constant field for the CdF$_2$:Ga crystal.

For temperature dependent studies (400 K-200 K) the Chemomagnetics RKC-REX-C1000 temperature control system was connected to the probe through the top end of the magnet. This system used conditioned air blown by the FTS Systems Air-Jet. The REX-C1000 was set to the desired temperature, and once this temperature was reached, the sample was left for at least one hour to ensure thermal equilibrium with the cooled (or heated) air.

3.5.4: Error Analysis

Origin 6.0 was used to plot the result of T_1 experiments and fit the experimental data to a single exponential recovery. The best error in the best fit lines was less than one percent in the majority of spin lattice relaxation times. In the cases where the error in was on the order of a few (1-2) percent, the best fit was too large around the "bend" of the exponential and too low in the tail of the exponential.

This indicates there is a not a single exponential and thus not a single T_1. There is a distribution of relaxation times most likely caused by and uneven distribution of dopants throughout the crystal. I tripled the error in the best fit curve to account for these errors in T_1.

The results of T_1 experiments plotted as function of reciprocal temperature for crystal were then plotted on a semi-log axis. Linear fits to data were added using Origin with the error in the slopes being relatively small (~3-9%) and excluding systematic laboratory errors such as a small, but not insignificant, temperature gradient between the sample and temperature control unit's sensor. My estimation of this temperature gradient is ± 1 K based on the short distance (2-3 mm) between the sensor and sample. The following procedure was used to get a better idea of the true experimental error. Best fit lines were drawn in by hand to represent the "extreme" best fits i.e. best fit lines using the maximum and minimum slopes as determined by the eye. These slopes were compared to the slope of the best fit line generated by Origin using

$$3.1 \qquad \% \text{ error} = \frac{\left| slope_{eye} - slope_{Origin} \right|}{slope_{Origin}} 100\%$$

This gave very pessimistic values for the percent error. However, I believe this method was more accurate than just using best fits to functions. This procedure gave 10% error for the temperature dependent ^{19}F data and 7% error for the temperature dependent ^{113}Cd data.

4. Host and Impurity NMR Data

Section 4.1: Host NMR – ^{113}Cd Relaxation Versus Temperature
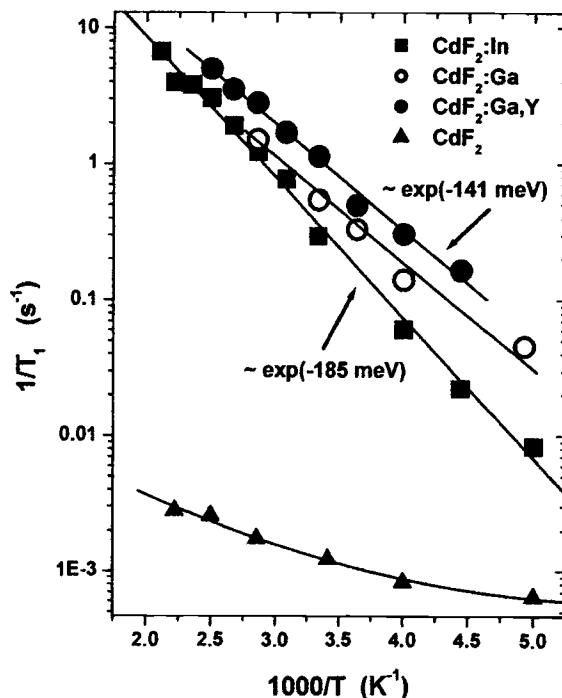
Figure 4.1: Relaxation rate versus reciprocal temperature of ^{113}Cd.

Temperature dependent ^{113}Cd relaxation measurements were done on the CMX-360 spectrometer in a field of 8 Tesla. The data from the undoped and indium-doped crystal were collected by Mark Shroyer (Shroyer et all, 2002). The data for the dopecd crystals exhibit Arrhenius behavior when plotted versus reciprocal temperature on a semi-log scale. It is evident that all of the doped crystals exhibit an enhanced relaxation compared to the undoped crystal. From the Arrhenius behavior a characteristic activation energy of 185 ±10 meV for the indium-doped crystal and 141 ± 10 meV for both of the codoped and Ga doped crystals has been

extracted. The activation energy for the indium-doped crystals is greater than both
of the gallium-doped crystals over this temperature range. Also, both of the
gallium-doped crystals exhibit the same activation energy within experimental
error.

Section 4.2: Host NMR – ^{19}F Relaxation Versus Temperature
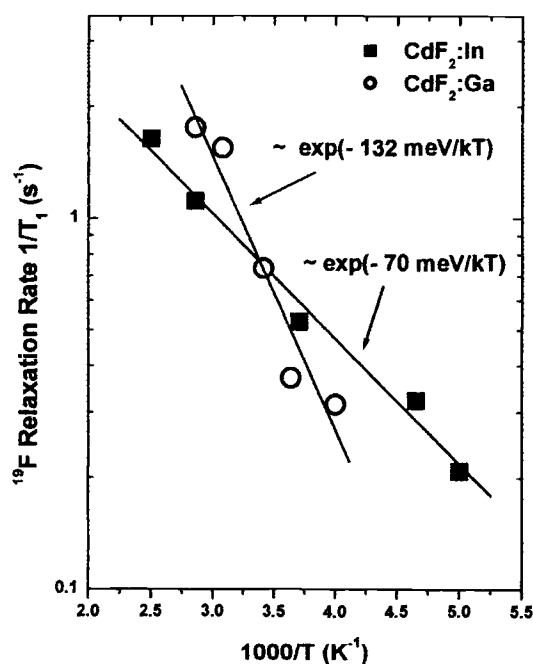
Figure 4.2: Relaxation rate versus reciprocal temperature of ^{19}F.

Temperature dependent ^{19}F relaxation measurements were done on the CMX-360
spectrometer in a field of 8 Tesla. These data also exhibit Arrhenius behavior over
this temperature range giving a characteristic activation energy of 132 ± 13 meV
for the gallium-doped crystal and 70 ± 10 meV for the indium-doped crystal. The
^{19}F activation energy is larger for the gallium-doped crystal compared to the
indium-doped crystal. This behavior differs from the ^{113}Cd relaxation data.

Section 4.3: Host NMR – ¹⁹F Relaxation Versus Applied External Field
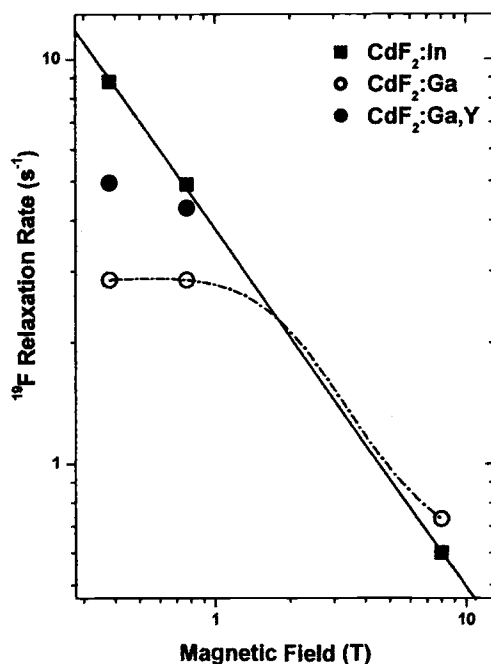
Figure 4.3: Relaxation rate versus external field of ¹⁹F.

The low-field data were taken on the hand-built spectrometer at room temperature. A field dependent relaxation for ¹⁹F is seen for all three crystals. The indium-doped crystal appears to exhibit a linear field dependence on the log-log plot. Both of the gallium-doped crystals change their field dependence over this range of external fields, becoming less field dependent at lower applied fields. The curve for the gallium-doped crystal is intended just to guide your eye. There is no functional form to the curve.

Section 4.4: Impurity NMR – ^{69}Ga
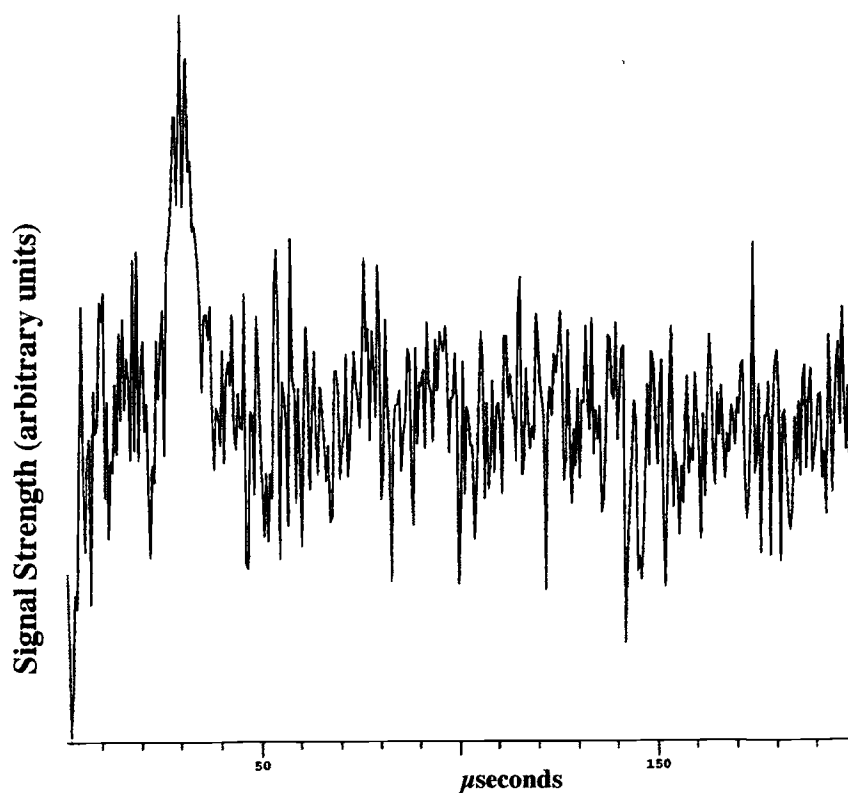
Figure 4.4: Spin echo of ^{69}Ga in an unreduced crystal.

The ^{69}Ga impurity was detected in an unreduced crystal using the technique of spin echoes at 293 K in an external field of 8 T. The same measurement was attempted in a reduced CdF_2:Ga crystal but no echo was detected. This is the first time the gallium has been directly observed in this material. Due to the low concentration of the gallium, a week of continual data acquisition was needed to extract the spin echo from the background noise. The spin echo shown above took approximately two million acquisitions.

5. Ga – DX Center Statistics

In this chapter we consider the thermal statistics of the DX (or negative U) model of CdF_2:Ga. Our approach investigates the average occupation of electrons in the conduction band and finds a thermally activated process for temperatures between 100 and 330 Kelvin. We also investigate the average population of the shallow donor state and find a thermally activated process for temperatures between 100 and 285 Kelvin.

Section 5.1: Structural Statistics of Interstitial Deep Donor Sites

Consider a lattice containing N_I neutral Ga impurities that initially behave as hydrogenic donors. With the assistance of an energy lowering lattice distortion together with acquisition of an electron from one of the donor impurities, Ga atoms migrate to one of six equivalent nearby interstitial lattice sites, leaving behind a vacancy and an equal number N_{sh}^+ of ionized Ga *atoms*. The process is described by the reaction

5.1 $$2N_{sh}^0 \leftrightarrow N_d^- + N_{sh}^+$$

where N_d^- is the interstitial. The right hand side will be treated as an interstitial-ion *pair* with the interstitial Ga *doubly* occupied. The negatively charged interstitial components are then double-donor sites which generally lie deep in the band gap. Thus we distinguish between *shallow (sh)* and *deep (d)* donors. It is assumed that the deep donor is stable only as a doubly negatively charged configuration.

Thus, as T -> 0° the impurity structure consists of

- $N_d^- = N_I/2$ deep donor-ionized donor *pairs*

- N_d^- vacancies

With increasing temperature deep donor-shallow ionized donor pairs recombine to produce two neutral shallow donors (Equation 5.1). Total impurity number conservation is given by

5.2
$$N_I = \left[N_d^- + N_{sh}^+ \right] + N_{sh}^0$$

where the brackets specify the deep donor-ionized shallow donor pairs. Since $N_d^- = N_{sh}^+$ we may also write

5.3
$$N_I = 2N_d^- + N_{sh}^0$$

The initial consideration is a process in which Ga atoms migrate to interstitial sites with an activation energy ε_A which requires a calculation of the average numbers of deep-ionized shallow donor pairs, N_d^-, and normally sited neutral (hydrogenic) shallow donor *atoms* N_{sh}^0 as a function of temperature and the deep-shallow *pair* activation energy. This is determined from the Grand Partition functions (Wasserman, 2004)

5.4
$$Z_{sh} = \left[1 + e^{-\beta(0-\xi_{sh})} \right]^{N_I}$$

5.5
$$Z_d = \left[1 + 6e^{-\beta(\varepsilon_A - \xi_d)} \right]^{N_I/2}$$

where the factor of six in equation 5.5 accounts for the six-fold interstitial degeneracy consistent with the LDA calculations of Park and Chadi and $\beta = 1/kT$. In Equation 5.4 ε_{sh} has been set to zero. This means ε_A is the deep-shallow pair activation energy. The site counting exponents N_I and $N_I/2$ are the number of sites available for each species. They assure at $T = 0°$

$$5.6 \qquad\qquad N_d = N_{sh}^{+} = N_I/2$$

is satisfied. Here ζ_{sh} is the chemical potential for neutral shallow donors and ζ_d is the chemical potential for deep donor-ionized donor *pairs* with, according to Equation 5.1,

$$5.7 \qquad\qquad 2\zeta_{sh} = \zeta_d.$$

Taking Equation 5.7 together with Ga atom conservation

$$5.8 \qquad\qquad N_{sh}^{0} + 2N_d^{-} = N_I$$

where N_d^{-} counts deep donor-ionized shallow donor *pairs*.

The mean number of any particle or occupation of sites can be found using

$\langle particle \rangle = \dfrac{1}{\beta}\dfrac{\partial}{\partial \mu_\gamma}\ln Z_\gamma$. Where the derivative is with respect to the appropriate

chemical potential and Z_γ is the appropriate partition function. With the constraints listed previously in Equations 5.6, 5.7 and 5.8, an equation for the chemical potential is created. Once the chemical potential is found, the number of shallow donors and deep sites in terms is found to be

$$5.9 \qquad N_{sh}^0 = \frac{\left(36e^{\beta\varepsilon_A}\right)^{1/3}}{6 + \left(36e^{\beta\varepsilon_A}\right)^{1/3}} N_I$$

$$5.10 \qquad N_d^- = \frac{3}{6 + \left(36e^{\beta\varepsilon_A}\right)^{1/3}} N_I$$

Section 5.2: Electron Statistics of Deep-Shallow Donor Sites

In this DX model the deep donor is stable only when it retains its negative charge (is doubly occupied). Therefore if an electron pair is thermally excited from the deep donor it must revert to a shallow donor (charged or uncharged) and conduction band excitations. The electron balance condition for determining concentrations is

$$5.11 \qquad N_I = \langle n_e \rangle + \langle n_{sh}^0 \rangle + \langle n_{dp}^- \rangle$$

where $\langle n_e \rangle$ is the average electronic occupation number of conduction band, $\langle n_{sh}^0 \rangle$ is the average occupation number for electrons on neutral shallow donor sites and $\langle n_d^- \rangle$ is the average occupation number of doubly occupied deep donor sites, i.e. deep donor-ionized shallow pairs. Assuming the non-degenerate conduction electron limit we can write immediately

$$5.12 \qquad \langle n_e \rangle = \sqrt{\frac{\pi}{2}} \left(\frac{m^*}{\beta\hbar^2}\right)^{3/2} e^{\beta\mu}$$

where μ is the electron chemical potential. To find $\langle n_{sh}^0 \rangle$ we begin with the grand partition function (Wasserman, 2004)

5.13
$$Z_{sh} = \left[1 + 2e^{-\beta(\varepsilon_{sh}-\mu)}\right]^{\left[N_{sh}^0 + \left(2N_d^- - \langle n_{dp}^- \rangle\right)\right]}$$

where N_{sh}^0 is the temperature dependent number of neutral shallow donor sites given in Equation 5.9 and ε_{sh} is the doubly degenerate neutral shallow donor energy level measured from the conduction band minimum. However, the number of shallow sites is coupled to electron pair excitations from the deep donor. This is accounted for by the additional terms in the exponent.

To find $\langle n_{dp}^- \rangle$ we write the grand partition function (Wasserman, 2004)

5.14
$$Z_{dp} = \left[1 + e^{-\beta(\varepsilon_{dp}-2\mu)}\right]^{\left[N_d^- - \langle n_{sh}^0 \rangle /2\right]}$$

where N_d^- is the temperature dependent number of deep donor sites given in Equation 5.10 and where ε_{dp} is the deep donor energy level (measured from the conduction band minimum). In the "negative U" model, the energy consists of two contributions,

5.15
$$\varepsilon_{dp} = 2\varepsilon_{sh} - |U|$$

in which $-|U|$ is the effective attraction between two electrons on the donor, taking into account the compensating energy associated with the lattice distortion.

The number of deep sites is coupled to shallow donor excitations. This is accounted for by the additional term in the exponent. What then follows is the pair of coupled equations for $\langle n_{sh}^0 \rangle$ and $\langle n_{dp}^- \rangle$

5.16
$$\langle n_{sh}^0 \rangle = \frac{1}{\beta}\left[N_{sh}^0 + \left(2N_d^- - \langle n_d^- \rangle\right)\right]\frac{\partial}{\partial\mu}\ln\left[1 + 2e^{-\beta(\varepsilon_{sh}-\mu)}\right]$$

and

5.17
$$\langle n_{dp}^- \rangle = \frac{1}{\beta}\left[N_d^- - \langle n_{sh}^0 \rangle/2\right]\frac{\partial}{\partial\mu}\ln\left[1 + e^{-\beta(\varepsilon_{dp}-2\mu)}\right]$$

Finally, using Equations 5.9, 5.10, 5.11, 5.16, and 5.17 the chemical potential μ can be determined, from which $\langle n_e \rangle$ and $\langle n_{sh}^0 \rangle$ follow. These results are plotted for the values of $\varepsilon_{dp} = -340$ meV, $\varepsilon_{sh} = -120$ meV, $\varepsilon_A = -270$ meV, and $N_I = 10^{24}$ m^{-3} associated with Ga impurities.
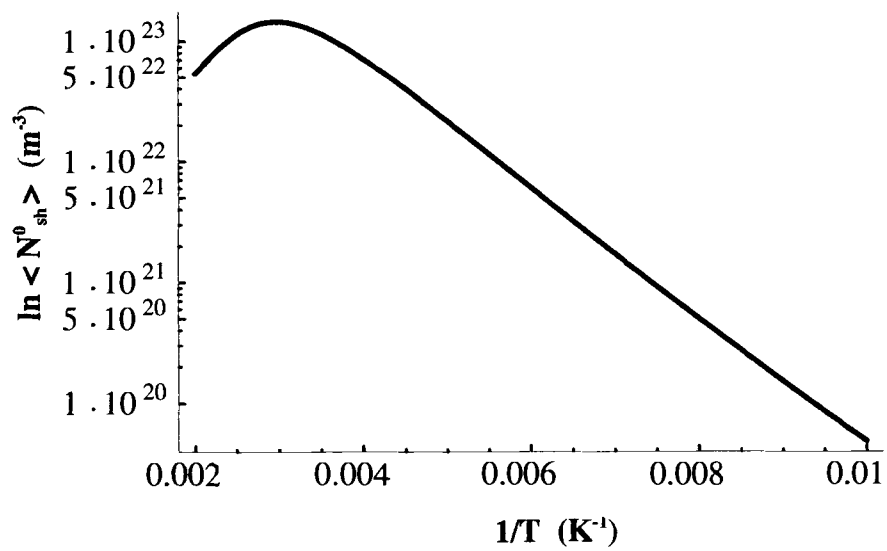
Figure 5.1: The mean number of shallow donors versus reciprocal temperature.
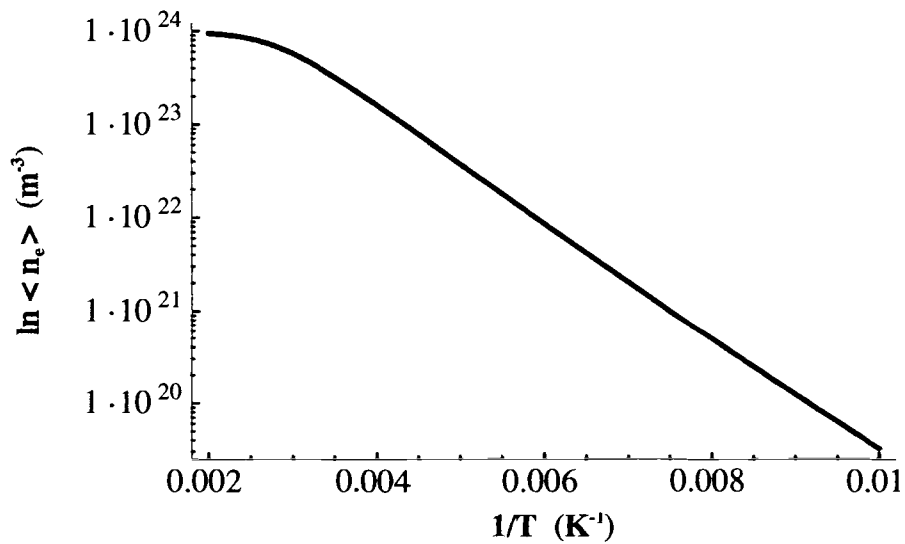
Figure 5.2: The mean number of conduction electrons versus reciprocal temperature.

In Figure 5.1 Arrhenius behavior is seen in the average number of shallow donors from 100 to approximately 285 Kelvin with an activation energy of 110 meV. As the temperature increases above 285 Kelvin, the average number of shallow donors continues to increase until roughly 330 Kelvin. At 330 Kelvin the population is at its maximum. This can be explained by the existence of enough thermal energy to completely ionize the shallow donor state faster than the shallow donor state can be created for temperatures above 330 Kelvin.

Arrhenius behavior is also seen in the average occupation of electrons in the conduction band (Figure 5.2) from 100 to approximately 330 Kelvin with an activation energy of 123 meV. Around 500 Kelvin the average occupation of electrons in the conduction band begins to saturate. This can be explained for temperatures of 500 Kelvin and above because average number of electrons in the conduction band is approaching the gallium doping level, with each gallium contributing one extra electron under the current model.

6. Analysis and Conclusions

Section 6.1: Characterization of CdF_2 Crystals from Optical Studies

Optical absorption spectra have been collected for the indium and gallium-doped

crystals at low (5-10 K) temperatures (Ryskin et al., 1998a; Ryskin et al., 1998b;

Shcheulin et al., 2001; Piekara et al., 1977). The energies obtained from these

spectra (Figure 6.1) have been associated with the transition of electrons from the

deep, DX state into the conduction band (given by the UV-visible peak) and the

transition of electrons from the shallow donor states into the conduction band

(given by the IR peak). These energies are 250 meV and 100 meV for the indium-

doped crystal and 340 meV and 120 meV for the gallium-doped crystal,

respectively (Shcheulin et al., 1999).
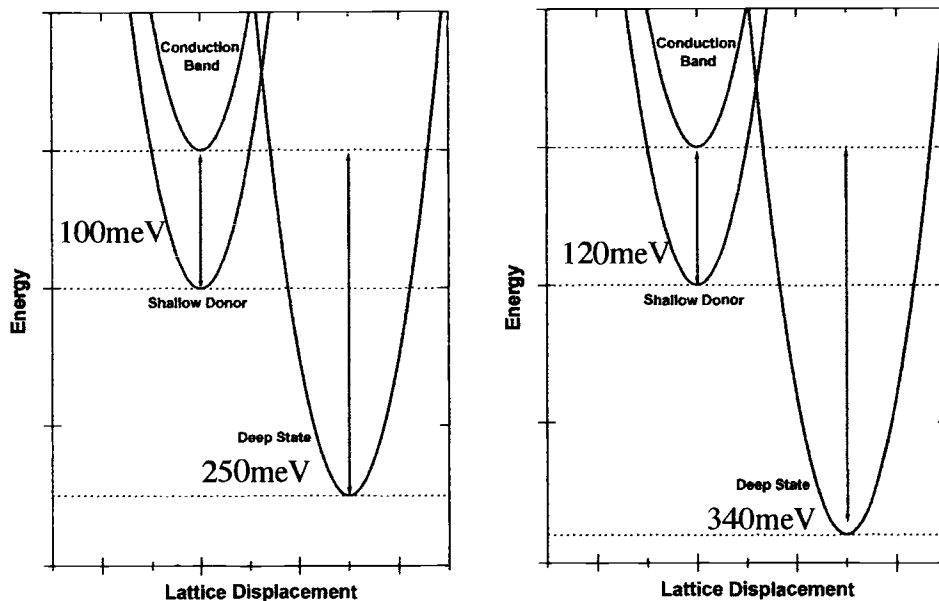
Figure 6.1: Transition energies obtained from optical studies of CdF_2:In (left) and CdF_2:Ga (right).

Two remarks about these results need to be emphasized. Firstly, these results give specific transition energies under the current model. These transition energies cannot be compared directly to the activation energies from the NMR relaxation experiments. The NMR activation energies are "average" or "characteristic" energies. They are not a particular energy in the current model. The statistical treatment of the three level system must be done before comparing the energies between the NMR and absorption experiments. This was done for the indium-doped crystal (Shcheulin et al., 2001), resulting in very good agreement between the two experimental methods (Shroyer, 1999). In the statistical results, the plots of the natural log of the population of shallow donors versus reciprocal temperature and the natural log of the concentration of conduction electrons versus reciprocal temperature exhibit almost perfect Arrhenius behavior. From these graphs, activation energies were calculated. The NMR activation energy from ^{19}F relaxation experiments was attributed to dipole-dipole interactions with shallow donors and spin diffusion with other fluorines and had a value of 70 ± 10 meV compared to 74 meV from the statistical treatment. The NMR activation energy from [113]Cd relaxation experiments was attributed to hyperfine fluctuations in the cadmium's local field due to conduction electrons and had a value of 185 ± 10 meV compared to 195 meV from the statistical treatment. Thus the NMR experiments for indium-doped crystals are consistent with the results of the absorption experiments and theoretical calculations based on the current model.

Secondly, the results from the optical and metastability (Shcheulin et al., 2001) studies suggest that the transition energies of the gallium-doped crystal are consistently larger that those of the indium-doped crystal. In the metastability studies, the critical temperature was 200 K for CdF_2:Ga and 70 K CdF_2:In. This increase in the critical temperature is indicative of larger energies in CdF_2:Ga. From this we expect the activation energies from the NMR experiments on the gallium-doped crystal to be consistently larger than those from the indium-doped crystal. We also have no reason to believe the statistical treatment of the system would not agree with the NMR results. However, these calculations have not been done previously for the gallium-doped crystal, but were done as part of this work.

Section 6.2: Analysis of ^{113}Cd Relaxation Versus Temperature

We attribute the relaxation of ^{113}Cd to the presence of electrons in the conduction band. This is strongly suggested by the similarity to the results of the indium-doped NMR experiments and statistical calculations (Shroyer, 1999). The relaxation of ^{113}Cd is definitely associated with doping of CdF_2. The relaxation rate for the doped crystals is much faster then the relaxation rate of the undoped crystal. The process of doping introduces extra electrons into the material and the reducing process frees the extra electrons by (at least partially) removing fluorine interstitials which trap the extra electrons from the dopants. The relaxation is further enhanced in the CdF_2:Ga by codoping with yttrium. The codoping is

believed to increase the number of active shallow donors (thus increasing the number of electrons in the conduction band) (Kazanskii, 2000).

A rough calculation of $\dfrac{1}{T_1}$ at room temperature can be made by using equation 2.14 and compared to our experimental results. Using $N = 10^{18}$ electrons per cubic centimeter and $|\phi(0)|^2 = 10^{25}$ per cubic centimeter the relaxation rate was found to be 0.025Hz. This is not unreasonable when compared to 0.7 Hz for CdF_2:Ga. To further check this rough estimation, a rough value of $|\phi(0)|^2$ was found using atomic data (Carter et al., 1977) to be $|\phi(0)|^2 = 4.5 \times 10^{25}$ per cubic centimeter. Using this value in equation 2.14 gives a room temperature relaxation rate of 0.5 Hz. While these calculations only estimate the relaxation rate they are of the same order of magnitude.

Further support for the relaxation of ^{113}Cd by conduction electrons can be found theoretically by examining the Hamiltonian of an electron in a magnetic field. The Hamiltonian is given by (Cohen-Tannoudji, 1977)

$$6.1 \qquad \mathcal{H} = \frac{1}{2m_e}\left[\vec{P} - q\vec{A}_I(\vec{R})\right]^2 + qU(\vec{R}) - 2\mu_B\left(\frac{\vec{S}}{\hbar}\right)\cdot\vec{\nabla}\times\vec{A}_I(\vec{R})$$

The terms in the magnetic hyperfine Hamiltonian include the coupling of the magnetic moment of the nuclei with the orbital angular momentum of the electron (those linear in magnetic vector potential which is assumed small), and a term that is proportional to the square of the vector potential (which is assumed very small

and dropped). Of the terms that are linear in the vector potential, the "contact term" is of particular relevance to this work. The "contact term" is the contribution of the internal field of the nuclei which interacts with the electron and is given by

$$6.2 \qquad \mathcal{H}_{hf,contact} = \frac{8\pi}{3}\gamma_e\gamma_n\hbar\delta(r_1)(\vec{I}\cdot\vec{S})$$

$\left\langle\varphi_{k,l,m,\varepsilon}\left|\mathcal{H}_{hf,contact}\right|\varphi_{k',l',m',\varepsilon'}\right\rangle$ is related to the spin-lattice relaxation rate, $\frac{1}{T_1}$ given by equation 2.14. The important part is

$$6.3 \qquad \frac{1}{T_1} \propto \left|\left\langle\varphi_{k,l,m,\varepsilon}\left|H_{hf,contact}\right|\varphi_{k',l',m',\varepsilon'}\right\rangle\right|^2 \propto \left(\left|\phi_e(0)\right|^2\right)^2$$

Equation 6.3 basically states that the relaxation rate is related to the probability of the electron at the nucleus. In CdF_2 the expectation value in equation 6.3 will be nonzero only if both states are s-states. Furthermore the coupling increases with the nuclear charge, Z. Z is equal to 48 for cadmium and 9 for fluorine. Relaxation by conduction electrons clearly favors cadmium over fluorine.

Our [113]Cd relaxation data exhibit Arrhenius behavior from 200 K to 400 K. The activation energy associated with this behavior is 141 ± 10 meV for both of the gallium-doped crystals and 185 ± 10 meV for the indium-doped crystal. Additionally, the statistical treatment of the three level system (Wasserman, 2004) shows Arrhenius behavior from 100 to approximately 330 Kelvin and gives an activation energy of 123 meV for a gallium-doped crystal. These activation energies for the gallium-doped crystals are very surprising because both the theoretical and experimental energies are less than the activation energy of the

indium-doped crystal, contrary to our expectations discussed above. It is also interesting to note that our theatrical treatment suggests the carrier concentration is not entirely thermally activated above 330K. Around 500K the carrier concentration appears to begin to saturate. The lower than expected activation energies led us to investigate the relaxation of ^{19}F as a check for the consistent increase in energies between the gallium and indium-doped crystals.

It should also be noted that a state between the shallow donors and deep state was once proposed (Ryskin et al., 1998a; Ryskin et al., 1998b). It seems our relaxation data and statistical treatment (Wasserman, 2004) indicate further investigation into this intermediate state is needed. The mention of this intermediate state disappears in later articles but may help reconcile the residual differences between our measurements for ^{113}Cd and expectations from the optical results.

Section 6.3: Analysis of ^{19}F Relaxation Versus Temperature

Spin-lattice experiments from 200 K to 400 K were carried out on ^{19}F to further investigate the observed increase in energies between CdF_2:In and CdF_2:Ga from the optical data. From the NMR data, the activation energy from CdF_2:Ga was larger than the activation energy from CdF_2:In. This behavior was also seen by the optical experiments. The gallium-doped crystal's energy was roughly twice as big as the indium-doped crystal's energy. This is roughly the scaling observed by Ryskin's group (Kazanskii, 2000).

In NMR experiments done on CdF_2:In (Shroyer, 1999), the differences between the relative activation energies between the ^{19}F and ^{113}Cd suggested that the host nuclei were being relaxed through different processes. The fluorine relaxation was attributed to dipolar interactions between localized (shallow donor) spins and ^{19}F ions through via spin diffusion. Spin diffusion in this material works as follows. A shallow donor relaxes a neighboring fluorine ion. This ion can then relaxes one of its neighboring fluorine ions through a mutual spin flip. This process continues so that the shallow donor's relaxation can be "communicated" to fluorines which are not its neighbors.

Spin diffusion is very effective for the fluorine lattice. ^{19}F is 100% isotopically abundant and has a large gyromagnetic ratio (over 4 times larger than ^{113}Cd). Furthermore, only about 25% of the cadmium ions even have a magnetic moment and cadmium ions are roughly twice as far apart from each other in the crystal structure. This does not take into account the distance between cadmium ions that both possess a magnetic moment, only the shortest distance (and thus strongest dipole-dipole interaction) between cadmium ions. This process is therefore very ineffective for the cadmium nuclei. ^{113}Cd relaxation was attributed to hyperfine interactions with conduction electrons.

We could not, however, readily attribute the relaxation of ^{19}F to any specific mechanism due to the similarity of the activation energies (E_{ac}) between ^{19}F and ^{113}Cd in CdF$_2$:Ga. Recall that E_{ac} is 141 ± 10 meV for ^{113}Cd and 132 ± 13 meV for ^{19}F. This similarity of the fluorine and cadmium activation energies brings up the possibility that both host nuclei are being relaxed by conduction electrons. To investigate this further, I examined fluorine relaxation as function of applied external field.

Section 6.4: Analysis of ^{19}F Relaxation Versus Applied External Field

Field dependent spin-lattice experiments were done on ^{19}F in the gallium-doped crystal at fields of 0.38 , 0.77, and 8 Tesla using the standard inverting π, $\pi/2$ pulse sequence. Field dependent experiments were also done on the codoped crystal using the same pulse sequence at fields of 0.38 and 0.77 Tesla. There is a clear dependence of the spin-lattice relaxation rate over this range of applied external fields. However, the field dependence is not constant over this range of applied fields. In CdF$_2$:Ga there seems to be a regime of field independence for external fields less than roughly 1 Tesla.

The relaxation rate of ^{19}F by conduction electrons will not depend on our applied magnetic fields. With the correlation function for hyperfine field fluctuations being proportional to an exponential recovery

6.4
$$G(t) = G(0)e^{-\frac{t}{\tau}}$$

the Fourier transform of this called the spectral function

6.5
$$J(\omega) = \int_{-\infty}^{\infty} G(t)e^{-i\omega t} dt$$

this function is proportional to the transition rate between spin states of a nuclei (Slichter, 1980). The spectral function is proportional to a Lorentizian, namely

6.6
$$J(\omega) \propto \frac{2\tau}{1 + \omega^2\tau^2}$$

Assuming a strong static field in the z-direction the spin-lattice relaxation rate is

6.7
$$\frac{1}{T_1} = 2\gamma_N^2 \frac{\langle b_o^2 \rangle}{3} \frac{\tau}{1 + \omega^2\tau^2} \propto J(\omega)$$

Where b_o can be either $\pm b_q$, the values of the magnetic field caused by an electron as it transitions from one orientation to another, ω is the Larmor frequency and τ is the time in which it takes b_o to oscillate. The important part being that the spectral function is related to the relaxation rate.

If $\omega\tau$ is small the relaxation rate is independent of magnetic field. For large $\omega\tau$ the relaxation rate is proportional to ω^{-2}. The transition between these two types of behavior is when $1 \cong \omega^2\tau^2$ which defines the cutoff frequency

6.8
$$\omega_{cuttoff} \cong \frac{1}{\tau}$$

The fluctuations of the local hyperfine fluctuations due to conduction electrons ($\tau \approx 10^{15}$ s) are fast compared to the precession of the fluorine's moment. When

looking at the spectral function of these rapid fluctuations, the Larmor frequencies

associated with our field lie well away from the cutoff frequency of the fluctuating

hyperfine field (Figure 6.2).
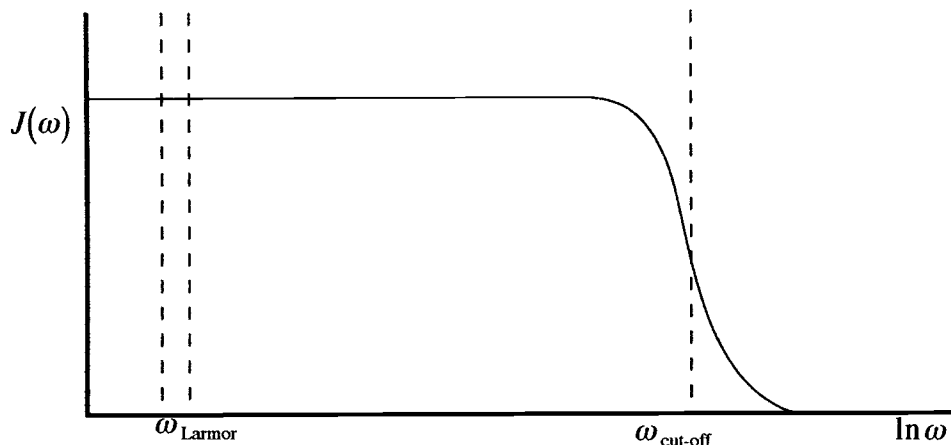
Figure 6.2: Spectral function of hyperfine
fluctuations and ^{19}F's Larmor frequencies.

The dependence of the spin-lattice relaxation rate of ^{19}F on the applied field rules

out conduction electrons as the cause of the relaxation. By ruling out conduction

electrons as a relaxation mechanism for ^{19}F, we attribute the relaxation to the

presence of unpaired spins associated with the shallow donor state. To further

explore this claim, ^{19}F relaxation will have to be carried out on CdF_2:Ga,Y from

200 K to 400 K. This crystal should show and enhanced T_1 compared to CdF_2:Ga

for our conclusion to remain consistent with the presence of more active

impurities.

The field dependence of ^{19}F in CdF$_2$:Ga and CdF$_2$:Ga,Y is not independent of field over our range of applied external field. It is interesting to note that for applied fields of less than one Tesla the relaxation rate of the gallium-doped crystal is practically independent of field. The only model that accounts for this behavior is for limited diffusion. Recall, that for this case the relaxation rate is independent of external field for $\omega\tau \ll 1$ but has a field dependence of $B^{-\frac{1}{2}}$ for $\omega\tau \gg 1$ (see Table 2.1). More field dependent measurements must be done on both gallium-doped crystals before the field dependence at upper end of applied external field can be found and compared to this model. When compared to the field dependence of CdF$_2$:In it is clear the indium-doped crystal is not in this crossover regime. Its field dependence is linear on this scale over the entire range of fields.

The cut-off frequency can be estimated from Figure 4.3 for CdF$_2$:Ga to be around 2.5 Tesla. Using equation 6.8 this puts the electronic fluctuation time at roughly 2.3 picoseconds. In the case of CdF$_2$:In, the cut-off frequency is not seen over the same range of fields. Using 0.1 Tesla as the lower bound on the magnetic field an upper bound on the electron's fluctuations can be found to be approximately 60 picoseconds.

Arrhenius behavior from 100 to approximately 285 Kelvin was seen in our statistical treatment of the three level system (Wasserman, 2004) giving an activation energy of 110 meV. Additionally this model predicts a maximum

concentration of shallow donors around 330K. Above 330K thermal excitations are assumed to completely ionize the shallow donors which decreases their population. Our theoretical activation energy is roughly 20% lower than our activation energy of 132 ± 13 meV. However, our statistical treatment gives an activation energy that is larger, as was expected based on optical data, than the activation energy from the statistical treatment for the indium-doped crystal, but not valid over the entire range of our experimental data. Our model predicts thermal activation only until 285K not 400K. It is also interesting to note that the energies from our statistical treatment are lower than our experimental results for both ^{113}Cd and ^{19}F.

Section 6.5: Analysis of ^{69}Ga Spin Echo

Measurements on the gallium impurity were done at room temperature and with an applied field of 8 Tesla. A spin echo sequence was used on the unreduced sample and the codoped sample. The spin echo was only seen in the unreduced sample. However, the reducing process may itself be responsible for inability to observe the spin echo in the codoped sample. By reducing the material, shallow donor states and deep double donors are created as electrons trapped by interstitial fluorines are freed. The deep donors are theorized to move into an adjacent fluorine cube. This means there are six possible cubes the donor could move into. This could cause the single echo in the unreduced crystal to split into three separate resonances causing the intensity of each resonance to be less than that of

the single echo in the unreduced crystal. Losing signal will make observing the impurity that much more difficult. Many more acquisitions would be needed to see the spin echo in the reduced crystal if the resonance is being split.

Additionally, the presence of an electron in the shallow donor state will cause the gallium relaxation to be too fast to detect. If the statistical treatment of the gallium-doped crystal is related to the treatment of the indium-doped crystal only about 10% of the dopants will fall into this category. While not a large number, loosing any fraction of the impurity (already at the threshold for detection by NMR) is significant. Spin echoes should be done at low temperature in the reduced crystal to increase the number of deep states and increase the chance of observing the spin echo.

Section 6.6: Summary

The spin-lattice relaxation studies described in this thesis have determined the thermal activation energies for the concentrations of species that govern the electronic and optical properties of gallium-doped CdF_2.

The relaxation of ^{113}Cd was attributed to the concentration of electrons in the conduction band. The Arrhenius behavior of temperature dependent relaxation measurements on ^{113}Cd and gives an activation energy of 141 ± 14 meV. The statistical treatment of the system (Wasserman, 2004) gives an activation energy of 123 meV over the range of 100 to 330K. When our experimental results are

compared to similar measurements done on CdF_2:In, an activation energy of 185 ± 10 meV was measured. CdF_2:Ga was expected to exhibit larger energies compared to CdF_2:In based on optical and magnetic experiments. Thus it was surprising to see the ^{113}Cd's activation energy for the gallium-doped crystal was smaller than the indium-doped crystal's energy. However, we have found from our statistical calculations that the smaller activation energy is consistent with the optical excitation energies.

The Arrhenius behavior of temperature dependent relaxation measurements on ^{19}F gives an activation energy 132 ± 13 meV. The similarity between the activation energies of ^{113}Cd and ^{19}F in CdF_2:Ga did not allow us to attribute the relaxation of the fluorine to the presence of shallow donors, as was the case for CdF_2:In. Field dependent relaxation measurements were carried out on ^{19}F to explore the possibility of relaxation by conduction electrons. Field dependence was seen in the relaxation of the fluorine allowing the relaxation to be attributed to the presence of shallow donors. The statistical treatment of CdF_2:Ga using mean field theory (Wasserman, 2004) predicts Arrhenius behavior of the shallow donors with an activation energy of 110 meV over the range of 100 to 285K. This is much lower than my experimental results. However this energy is larger than the ^{19}F activation energy from CdF_2:In as was expected based on optical experiments.

Impurity NMR measurements were attempted on ^{69}Ga using the spin echo technique. The echo was only seen in the unreduced material. This is the first time the impurity has been observed directly in this material. To observe the spin echo two million acquisitions were needed.

BIBLIOGRAPHY

Abragam, A., (1985) Principles of Nuclear Magnetism, Oxford Science Publications.

Carter, G. C., Bennett, L. H., and Kahan, D. J., (1977) Metallic Shifts in NMR, Pergamon Press.

Cohen-Tannoudji, Claude, Diu, Bernard, and Laloë, Franck, (1977) Quantum Mechanics, Wiley-Interscience.

Fukushima, Eiichi, and Roeder, Stephen B. W., (1981) Experimental Pulse NMR: A Nuts and Bolts Approach, Addison-Wesley.

Kazanskii, Sergei, (2000) personal communication.

Park, C. H., and Chadi, D. J., (1999) Phys. Rev. Lett., **82**, 113.

Piekara, U., and Langer, J. M., and Krukowska-Fulde, B., (1977) Solid State Commun., **23**, 583.

Ryskin, A. I., and Fedorov, P. P., (1997) Phys. Solid State, **39**, 943.

Ryskin, A. I., and Shcheulin, A. S., Koziarska, B., Langer, J. M., and Suchocki, A., Buczinskaya, I. I., Fedorov, P. P., and Sobolev B. P., (1995) Appl. Phys. Lett.,**67**, 31.

Ryskin, A. I., Shcheulin, A. S., and Miloglyadov, E. V., Linke, R. A., and Redmond, I., Buchinskaya, I. I., Fedorov, P. P., and Sobolev, B. P., (1998a) Journal of Applied Physics, **83**, 2215.

Ryskin, A. I., Shcheulin, A. S., and Onopko, D. E., (1998b) Phys. Rev. Lett., **80**, 2949.

Shcheulin, A. S., Kupchikov, A. K., Angervaks, A. E., Onopko, D. E., and Ryskin, A. I., Ritus, A. I., Pronin, A. V., and Volkov, A. A., Lunkenheimer, P., and Loidl, A., (2001) Phys. Rev. B., **63**, 205207.

Shcheulin, A. S., Kupchikov, A. K., and Ryskin, A. I., (1999) Phys. Solid. State, **41**, 1444.

Slichter, C. P., (1980) Principles of Magnetic Resonance, Springer-Verlag.

Shroyer, M., (1999) thesis (unpublished), Oregon State University.

Shroyer, M., Warren, Jr., W. W., and Ryskin, A. I., (2002) Phys. Rev. B, 65, 165202.

Suchocki, A., Koziarska, T., Langer, T., Langer, J. M., (1997) Appl. Phys. Lett., 70, 2934.

Van Kranendonk J., (1954), Physica, 20, 781-800.

Warren, W. W., and Norberg, R. E., (1967) Phys. Rev, 154, 277.

Wasserman, Allen, (2004), personal communication.

Wilamowski, Z., Dmochowski, J., and Jantsch, W., (1997) Materials Science Forum, 258-263, 1443

APPENDICES

Appendix A: Statistical Treatment

Below is the Mathematica code created for the statistical treatment of CdF_2:Ga.

<<Graphics `Graphics`

Atom Considerations:

Clear[hb, kb, m, ß, εp, εa, nI, zp, zd, z0, np, npx, nd,

ndx, npd1, npd11, npd12, nsd1, ζp, ζa, λd, λp, λp1, λpx1, λvs, τ, t]

Grand Partition Function for Ga Impurities:

zp = (1+E^(-ß(0-ζp)))^(nI)

Grand Partition Function for Interstital-Ion Pairs:

zd = (1+6E^(-ß(εa-ζa)))^(nI/2)

Clear[nd]

npx=np-(1/ ß)D[Log[zp], ζp]

Clear[np]

ndx=nd-(1/ ß)D[Log[zd], ζa]

npd1={np, nd} /. Solve[{npx==0, ndx==0}, {np, nd}]

npd11=npd1 /. {ζa -> 2ζp}

npd12=npd11 /. {ζp -> (1/ ß)[Log[λp]} //Simplify

Ga Atom Balance:

nPD=(nI-npd12[[1]][[1]]-2npd12[[1]][[2]]) //Simplify

Solve For Chemical Potential:

λp1 = λp /. Solve [nPD == 0, λp]

λ1 = λp1[[2]]

np1=npd12[[1]][[1]] /. {λp -> λ1} //Simplify

nd1=npd12[[1]][[2]] /. {λp -> λ1} //Simplify

nsp1=np1 /. {nI -> 1} //Simplify

nsd1=nd1 /. {nI -> 1} //Simplify

Electron Considerations:

Clear[hb, kb, m, ß, εp, εd, nQ, nI, λ, λe, λe1, λc, μA, μB, zA, zD, nA, nD,

nc, ncε, ncc, nd1s, np1s, nAD1, nAx, nDx, nAD12, nAD13, t, τ]

Grand Partition Function for Shallow Donors:

zA = (1 + 2E^(-ß(εp-μA)))^(np1s+(2 nd1s-nD)) //Simplify

zD = (1 + E^(-ß(εd-2 μA)))^(nd1s-(na/2)) //Simplify

Average Occupation Number for Shallow Donors:

Clear[nd1s]

nAx = nA-(1/ß) D[Log[zA], μA]

Average Occupation Number for Deep Donor-Ion Pairs:

Clear[np1s]

nDx=nD-(1/ß) D[Log[zD], μA]

nAD1={nA, nD} /. Solve[{nAx == 0, nDx == 0}, {nA, nD}]

nAD12=nAD1 /. {μA -> (1/ ß)Log[λ], nd1s -> nd1, np1s -> np1} //Simplify

Average Occupation Number for Non-Degenerate Conduction Electrons:

nc = nQ λ

Number Balance for Electrons:

nc ε = (nc+nA12[[1]][[1]]+nAD12[[1]][[2]] -nI) /. {μA -> (1/ß) Log[λ] } / /

Simplify

ncn=Numerator[Together[nc ε]]

Solve for Chemical Potential:

λe1= λ /. {Solve[ncn==0, λ]}

λ1= λe1[[1]][[1]]

Conduction Electron Concentration:

ncc=nc /. { λ -> λ1};

nAD13=nAD12 /. { λ -> λ1};

Average Occupation Number for Shallow Donors:

nA1 = nA /. {μA -> (1/ß) Log[λc]} / / Simplify

Average Number of Ionized Sites:

n01=nd1+(np1-nA1) / / Simplify

Parameters:

hb = 1.05459 10^ (-34)

kb = 1.38066 10^ (-23)

m = 9.10953 10^ (-31)

ß = (1/ kb*t)

evtoJ = 1.60219 10^ (-19)

εp = -0.12*evtoJ

εd = -.340*evtoJ

εa=-0.270*evtoJ

nQ = Sqrt [(π /2)](m/(ß hb^2))^(3/2)

nI = 10^(24)

Plotting:

shen4 = LogPlot[Evaluate[ncc /. {t -> (1/τ)}], {τ, .01, .002}, AxesLabel ->

{"1/T", "ln(<ne>)"}, PlotPoints -> 500]

dshal4 = LogPlot[Evaluate[nA13[[1]][[1]] /. {t -> (1/τ)}], {τ, .01, .002},

AxesLabel -> {"1/T", "ln<nsh>"}, PlotPoints -> 500]

Display["lognesh.ai", shen4, "Illustrator"]

Display["lognsh.ai", dshal4, "Illustrator"]